PHILOSOPHICAL TRANSACTIONS OF THE ROYAL SOCIETY A MATHEMATICAL, PHYSICAL & ENGINEERING SCIENCES

Dipolar Oscillations and Phase Interferometry in Solid State n.m.r.

M. E. Stoll

Phil. Trans. R. Soc. Lond. A 1981 **299**, 565-584
doi: 10.1098/rsta.1981.0035

Phil. Trans. R. Soc. Lond. A **299**, 565–584 (1981)
Printed in Great Britain

Dipolar oscillations and phase interferometry in solid state n.m.r.

By M. E. Stoll
Division 8341, *Sandia National Laboratories, Livermore, California* 94550, *U.S.A.*

Dipolar modulation and phase interferometry, which are part of the class of high-resolution, double-resonance n.m.r. experimental techniques used to study solids, are examined in detail. A general theory of double-resonance interactions based on the heteronuclear dipolar Hamiltonian is presented. A number of experiments dealing with both heteronuclear and homonuclear dipolar modulation and selective dipolar difference spectra are discussed. These experiments are used to study hydrogen-bonded systems and catalytic systems. A simple theory explaining phase interferometry in n.m.r. is presented. Several phase interferometric experiments are also discussed. The motion and structure of ^{23}Na ions in β-alumina are examined with the use of this technique.

1. Introduction

During the period from 1970 to 1979 Professor Robert Vaughan and coworkers at the California Institute of Technology made many important contributions to the rapidly expanding field of solid state n.m.r. These contributions were widely varied and included development of a high-resolution 8-pulse cycle, cross polarization and dipolar oscillation techniques, phase-interferometric techniques, and techniques for studying nuclei with spins greater than $\frac{1}{2}$. Furthermore, these techniques were applied by Vaughan to study a host of physical systems, including single crystals, powders, hydrides, catalysts, amorphous materials and ionic conductors, by measuring chemical shift tensors, relaxation and dipolar interactions as a function of temperature, pressure and configuration. One could not possibly cover all of these topics adequately in the allotted space, so I have chosen to focus on the areas with which I am the most familiar: double resonance, including dipolar oscillations, and phase interferometry.

This paper will deal with some of the basic physics behind pulsed, double resonance and phase interferometry, as well as the initial and more recent applications of these techniques that have been carried out by the Vaughan research group in the last several years.

2. Double-resonance and dipolar oscillations

(*a*) *Background and theory*

Beginning with the cross-polarization decoupling experiments of Pines *et al.* (1973), there has been a renewed interest in nuclear magnetic double-resonance experiments. There had been, for quite a while, interest in liquid n.m.r. experiments utilizing continuous wave (c.w.) techniques like the nuclear Overhauser effect (n.O.e.) (Overhauser 1953) and spin tickling (Freeman & Anderson 1962). However, this resurgence was focused on pulsed methods in solids, particularly because of the wide range of applicability to the study of organic solids with the use of ^{13}C–^{1}H double-resonance techniques. In general I shall refer to ^{13}C as S spins and ^{1}H as I spins, both I and S equal to $\frac{1}{2}$.

The process of cross-polarization involves creating a transverse I magnetization and then spin-locking it with a parallel r.f. magnetic field in the rotating frame of the I spins, while applying an r.f. field in the rotating frame of the S spins. Transverse S magnetization will then grow parallel to the second r.f. field. The reason that this occurs is because of a characteristic modulation of the I–S dipolar interaction. Decoupling of I and S spins can be accomplished by irradiation of only the I spins while doing nothing to the S spins. In this case the I–S dipolar Hamiltonian has been modulated to become zero, hence the decoupling. Both of these are just specific cases of the more general I–S dipolar interaction.

Let us consider the most general Hamiltonian of two unlike spin $\frac{1}{2}$ nuclei (Stoll 1977). This is of the form

$$H_{IS,\,\text{general}} = a + \sum_i b_i I_i + \sum_j c_j S_j + \sum_{mn} d_{mn} I_m S_n, \tag{1}$$

where i, j, m and n are summed over values corresponding to x, y and z, and a, b_i, c_j, and d_{mn} are constants. Note that we have a total of 16 constants that are the coefficients of the 16 matrices that totally cover our 4×4 space. For convenience we choose our basis states as αα, αβ, βα, ββ or 1, 2, 3 and 4. The α and β refer to states having a z component of angular momentum of $+\frac{1}{2}$ and $-\frac{1}{2}$ and the first Greek letter refers to the I spin while the second refers to the S spin. A slight rewriting of this formula emphasizes the irreducible tensor concept:

$$H_{IS,\text{general}} = a + \boldsymbol{b}\cdot\boldsymbol{I} + \boldsymbol{c}\cdot\boldsymbol{S} + e\boldsymbol{I}\cdot\boldsymbol{S} + \boldsymbol{f}\cdot(\boldsymbol{I}\times\boldsymbol{S}) + \boldsymbol{g}\cdot(\boldsymbol{IS})\cdot\boldsymbol{h}, \tag{2}$$

where a, $\boldsymbol{b}$, $\boldsymbol{c}$, e, $\boldsymbol{f}$, $\boldsymbol{g}$ and $\boldsymbol{h}$ are a set of 17 constants of which only 16 are independent. The symbol $(\boldsymbol{IS})$ in (2) is understood to be the symmetric dyadic

$$(\boldsymbol{IS}) = \begin{bmatrix} I_xS_x & \frac{1}{2}(I_xS_y + I_yS_x) & \frac{1}{2}(I_xS_z + I_zS_x) \\ \frac{1}{2}(I_xS_y + I_yS_x) & I_yS_y & \frac{1}{2}(I_yS_z + I_zS_y) \\ \frac{1}{2}(I_xS_z + I_zS_x) & \frac{1}{2}(I_yS_z + I_zS_y) & I_zS_z \end{bmatrix}. \tag{3}$$

By setting (1) and (2) equal we get the relation

$$d_{ij} = \tfrac{1}{2}(g_ih_j + g_jh_i) + \delta_{ij}e + \sum_k \epsilon_{ijk}f_k. \tag{4}$$

Equation (2) shows the irreducible tensor character clearly because the terms $\boldsymbol{I}\cdot\boldsymbol{S}$, $\boldsymbol{I}\times\boldsymbol{S}$, and $(\boldsymbol{IS})$ will transform like spherical harmonics of zeroth, first and second order respectively. It turns out that all such I–S Hamiltonians can only cause four fundamental types of behaviour of the I or S magnetization: (1) no behaviour at all, (2) precession of magnetization, (3) linear oscillation of magnetization, and (4) transfer of magnetization between the I and S spins.

This first phenomenon, no behaviour at all, is not as trivial as it might first seem. In order to have no interaction between the I and S spins, we need to have a Hamiltonian that has all the constants of (1) equal to zero except a. We focus in particular upon making the $d_{mn} = 0$. Our I and S spins will interact via the heteronuclear dipolar Hamiltonian which, making the usual secular or truncated approximation, has the form

$$H_{IS(\text{secular})} = (\gamma_I\gamma_S/r^3)\,(1 - 3\cos^2\theta)I_zS_z, \tag{5}$$

where $\boldsymbol{r}$ is the internuclear vector, γ_1 and γ_S are the magnetogyric ratios and θ is the angle between $\boldsymbol{r}$ and the z-axis. So our strategy is to manipulate this Hamiltonian so that in the interaction frame of the r.f. radiation we have an average Hamiltonian of zero. We then can appeal to average Hamiltonian theory (Haeberlen & Waugh 1968; Rhim *et al.* 1974; Mehring 1976; Haeberlen 1976) which comes from the Magnus formulation of quantum mechanics (Magnus

PHILOSOPHICAL TRANSACTIONS OF THE ROYAL SOCIETY A MATHEMATICAL, PHYSICAL & ENGINEERING SCIENCES

1954). This theory says that, to first order, we can approximate the effect of a time-varying Hamiltonian by calculating the time evolution of the system under a time-invariant Hamiltonian which is just equal to the average Hamiltonian. Thus we apply r.f. radiation such that $\bar{H}_{IS}^{(0)} = 0$, where the bar and the superscript indicate the zeroth-order term of the Magnus expansion, which is just the average Hamiltonian. What 'decoupling' of I and S spins means then is that $\bar{H}_{IS}^{(0)} = 0$.

In the experiments of Hartmann & Hahn (1962) a well known double-resonance matching criterion was introduced:

$$\gamma_I H_{1I} = \gamma_S H_{1S}, \tag{6}$$

where H_{1I} and H_{1S} are the amplitudes of the I and S r.f. radiation. This was essentially just a condition in their c.w. experiment that gave $\bar{H}_{IS}^{(0)}$ a particular non-zero form. The proper generalization of this matching condition is that two spins will be coupled in any c.w. or pulsed experimen whenever $\bar{H}_{IS}^{(0)} \neq 0$ (Stoll *et al.* 1976*a*).

The second phenomenon that can happen owing to a general I–S Hamiltonian is precession of magnetization. If in our experimeut we have an average Hamiltonian of the form

$$\bar{H}_{IS}^{(0)} = \boldsymbol{b}\cdot\boldsymbol{I} + \boldsymbol{c}\cdot\boldsymbol{S}, \tag{7}$$

we know from the quantum theory of angular momentum that we will observe for any $\boldsymbol{I}$ magnetization a rotation or precession about an axis parallel to $\boldsymbol{b}$, and a precession about the axis parallel to $\boldsymbol{c}$ for any $\boldsymbol{S}$ magnetization. The angular frequencies of the precession will just be the lengths or magnitudes of the vectors $\boldsymbol{b}$ and $\boldsymbol{c}$.

The third phenomenon for a general I–S system is linear oscillation of the magnetization. The type of Hamiltonian giving rise to this behaviour is of the form

$$\bar{H}_{IS}^{(0)} = BI_zS_z, \tag{8}$$

where B is a constant. In this case it is useful to actually calculate the full behaviour. I shall use the density matrix formulation to calculate the quantum mechanical expectation value of the magnetization by the equation

$$\langle M(t)\rangle = \mathrm{tr}\,(\rho(t)\,M), \tag{9}$$

where ρ is the 4×4 density matrix describing our I–S spin system, the symbol tr means trace, and $M = I_x, I_y, I_z, S_x, S_y, S_z$. We can calculate, by using the Liouville equation for the evolution of the density matrix in the interaction frame (Slichter 1978),

$$\rho(t) = \exp(-\mathrm{i}\bar{H}_{IS}^{(0)}t)\,\rho(0)\exp(\mathrm{i}\bar{H}_{IS}^{(0)}t). \tag{10}$$

We now assume an initial density matrix of the form

$$\rho(0) = 1 + K_{I_x}I_x + K_{I_y}I_y + K_{I_z}I_z + K_{S_x}S_x + K_{S_y}S_y + K_{S_z}S_z, \tag{11}$$

by using the usual high-temperature approximation and keeping only terms linear in I or S, where the K_{I_x}, etc., are constants. This allows for any I and S longitudinal and transverse initial magnetization. Using (8), (10) and (11) we obtain

$$\begin{aligned}\rho(t) = {} & 1 + K_{I_x}\{I_x\cos(\tfrac{1}{2}Bt) + 2I_yS_z\sin(\tfrac{1}{2}Bt)\} + K_{I_y}\{I_y\cos(\tfrac{1}{2}Bt) - 2I_xS_z\sin(\tfrac{1}{2}Bt)\} + K_{I_z}I_z \\ & + K_{S_x}\{S_x\cos(\tfrac{1}{2}Bt) + 2S_yI_z\sin(\tfrac{1}{2}Bt)\} + K_{S_y}\{S_y\cos(\tfrac{1}{2}Bt) - 2S_xI_z\sin(\tfrac{1}{2}Bt)\} + K_{S_z}S_z.\end{aligned} \tag{12}$$

Using (9), (11) and (12) we can calculate the time development of the magnetization:

$$\left.\begin{aligned}&\langle I_x(t)\rangle = \langle I_x\rangle_0\cos(\tfrac{1}{2}Bt); \quad \langle I_y(t)\rangle = \langle I_y\rangle_0\cos(\tfrac{1}{2}Bt); \quad \langle I_z(t)\rangle = \langle I_z\rangle_0; \\ &\langle S_x(t)\rangle = \langle S_x\rangle_0\cos(\tfrac{1}{2}Bt); \quad \langle S_y(t)\rangle = \langle S_y\rangle_0\cos(\tfrac{1}{2}Bt); \quad \langle S_z(t)\rangle = \langle S_z\rangle_0.\end{aligned}\right\} \tag{13}$$

Note that the I_zS_z Hamiltonian of (8) causes the x and y components of I and S to oscillate linearly rather than precess, as for the Hamiltonian of (7). This means that if we should decouple the I and S spins at the point where $\cos(\frac{1}{2}Bt) = 0$, any initial x or y magnetization will have vanished! I shall return to this point later.

The fourth kind of behaviour that can occur is transfer of magnetization between the I and S spins. The Hamiltonian causing such transfer is of the form

$$\bar{H}^{(0)}_{IS} = BI_zS_z + CI_yS_y. \tag{14}$$

We assume an initial density matrix as in (11), and using (10) and (14) we compute

$$\begin{aligned}\rho(t) = 1 &+ K_{I_x}\{I_x\cos(\tfrac{1}{2}Bt)\cos(\tfrac{1}{2}Ct) + 2I_yS_z\sin(\tfrac{1}{2}Bt)\cos(\tfrac{1}{2}Ct) + S_x\sin(\tfrac{1}{2}Bt)\sin(\tfrac{1}{2}Ct)\\ &- 2I_zS_y\cos(\tfrac{1}{2}Bt)\sin(\tfrac{1}{2}Ct)\} + K_{I_y}\{I_y\cos(\tfrac{1}{2}Bt) - 2I_xS_z\sin(\tfrac{1}{2}Bt)\}\\ &+ K_{I_z}\{I_z\cos(\tfrac{1}{2}Ct) + 2I_xS_y\sin(\tfrac{1}{2}Ct)\} + K_{S_x}\{S_x\cos(\tfrac{1}{2}Bt)\cos(\tfrac{1}{2}Ct)\\ &+ 2S_yI_z\sin(\tfrac{1}{2}Bt)\cos(\tfrac{1}{2}Ct) + I_x\sin(\tfrac{1}{2}Bt)\sin(\tfrac{1}{2}Ct) - 2S_zI_y\cos(\tfrac{1}{2}Bt)\sin(\tfrac{1}{2}Ct)\}\\ &+ K_{S_y}\{S_y\cos(\tfrac{1}{2}Bt) - 2S_xI_z\sin(\tfrac{1}{2}Bt)\} + K_{S_z}\{S_z\cos(\tfrac{1}{2}Ct) + 2S_xI_y\sin(\tfrac{1}{2}Ct)\}.\end{aligned} \tag{15}$$

This quickly leads to the magnetization:

$$\left.\begin{aligned}\langle I_x(t)\rangle &= \langle I_x\rangle_0\cos(\tfrac{1}{2}Bt)\cos(\tfrac{1}{2}Ct) + \langle S_x\rangle_0\sin(\tfrac{1}{2}Bt)\sin(\tfrac{1}{2}Ct);\\ \langle I_y(t)\rangle &= \langle I_y\rangle_0\cos(\tfrac{1}{2}Bt);\\ \langle I_z(t)\rangle &= \langle I_z\rangle_0\cos(\tfrac{1}{2}Ct);\\ \langle S_x(t)\rangle &= \langle S_x\rangle_0\cos(\tfrac{1}{2}Bt)\cos(\tfrac{1}{2}Ct) + \langle I_x\rangle_0\sin(\tfrac{1}{2}Bt)\sin(\tfrac{1}{2}Ct);\\ \langle S_y(t)\rangle &= \langle S_y\rangle_0\cos(\tfrac{1}{2}Bt);\\ \langle S_z(t)\rangle &= \langle S_z\rangle_0\cos(\tfrac{1}{2}Ct).\end{aligned}\right\} \tag{16}$$

Equation (16) shows that a Hamiltonian like the one in (14) will cause x magnetization to be transferred oscillatorially between the I and S spins, while the y and z magnetizations merely oscillate as in the third phenomenon. For the special case of $B = C$, (14) gives the correct form for the usual cross-polarization Hamiltonian.

Many other Hamiltonians can be written, but they can all be transformed by rotations to look like one or more combinations of the four Hamiltonians mentioned here. These four effects represent the only kinds of behaviour that a coupled spin $\frac{1}{2}$ system can exhibit (Stoll 1977). Of course, complications arise when more than one of the types of Hamiltonian is present at the same time, and the exact time evolution of the magnetization can become very difficult to compute analytically. The situation can be made further complicated by considering a system with one S spin and several I spins. For certain Hamiltonians, however, the situation may fortunately still be analytically tractable (Stoll 1977). Unfortunately, there is not the space here to delve into that interesting and very often relevant case.

I now return to a ponit mentioned earlier when discussing linear oscillation. As stated, it is possible to allow the I–S interaction to act for a time until the transverse magnetization linearly oscillates to zero and then decouple the spins. At this point the magnetization will have vanished. This at first seems to violate some fundamental conservation law, perhaps conservation of energy. However, we can compute the energy of our system by taking

$$E(t) = \mathrm{tr}\,(\rho(t)\,H_{z+\mathrm{secular}\,IS}), \tag{17}$$

where $E(t)$ is the energy of the system as a function of time and

$$H_{z+\mathrm{secular}\,IS} = \omega_I I_z + \omega_S S_z + AI_zS_z. \tag{18}$$

PHILOSOPHICAL TRANSACTIONS OF THE ROYAL SOCIETY A MATHEMATICAL, PHYSICAL & ENGINEERING SCIENCES

Using (12) for $\rho(t)$ we find that $E(t)$ = constant, and energy is conserved. It is clear, though, that magnetization is not conserved. Magnetization does represent order, however, and order or entropy should be conserved. We can use the following equation to calculate the entropy, S, as a function of time:

$$S(t) = -k_{\mathrm{B}} \operatorname{tr}[\rho(t) \ln\{\rho(t)\}], \tag{19}$$

where k_{B} is the Boltzmann constant. When we use this equation we find that $S(t)$ = constant, and entropy is also conserved, as we would expect in a purely mechanical system of only two spins. Equation (12) shows that $\rho(t)$ for linear oscillation has some terms that are bilinear in I and S. These do not correspond to observable magnetization of either the I or S spin. For instance, the term $2I_yS_z \sin(\frac{1}{2}Bt)$ corresponds to $\langle I_yS_z\rangle \neq 0$, but we must remember that $\langle I_yS_z\rangle \neq \langle I_y\rangle\langle S_z\rangle$. This term corresponds to a correlation between I_y and S_z, and it essentially means that there is a strong probability of finding I along the $+y$ axis while S is along the $+z$ axis or of finding I along the $-y$ axis while S is along the $-z$ axis. Thus there is no net probability of finding I or S along any particular axis, yet I and S are correlated. This correlation represents a type of 'cross-product' ordering which creates a certain right or left 'handedness' or parity in the system. As might be expected, this parity has entropy associated with it, and the entropy of the parity is just what is needed to add to the entropy of the magnetization to give a constant total entropy. As time evolves the order is then passed back and forth between these two reservoirs.

We are now in a position to create a very simple physical picture of the effect of the I_zS_z Hamiltonian. The I spin sees a small magnetic field along the z axis due to the S spin. The I spin will precess about this magnetic field, but since at room temperature almost as many S spins are 'up' as are 'down', then half of the I spins precess clockwise and half counterclockwise. This leads to a net linear oscillation of the I spin due to both rotating and counter-rotating components. I stress, however, that this linear oscillation is due to statistical rather than quantum mechanical probabilities, unlike the linear oscillations due to phase interferometry discussed in §3.

Surprisingly, it turns out that in the fourth case, where magnetization is transferred between I and S and does not disappear, non-observable terms in the density matrix are still necessary for conservation of entropy. Equation (15) shows that for $\rho(t)$ we still have terms like I_yS_z. Thus, merely looking at the observable magnetization terms is insufficient for a full understanding of cross-polarization.

(*b*) *Experiments*

It has been shown by Pines *et al.* (1973) that one can obtain high-resolution ^{13}C n.m.r. data in many organic systems by cross-polarizing and then decoupling the ^{13}C from protons. The resulting spectrum is a chemical shift spectrum, which for a polycrystalline sample is a conventional powder pattern. Dipolar modulation is a two-dimensional type of experiment (Aue *et al.* 1976) whereby one varies the amount of dipolar contact between the ^{13}C and ^{1}H before acquiring the chemical shift spectrum. It was first shown by Hester *et al.* (1975*a*, *b*, 1976) and Waugh (1976) that one can obtain local structural information by (1) suppressing homonuclear dipolar couplings and (2) using the chemical shift tensor of a dilute spin species to orientate the heteronuclear dipolar oscillations. In general it is crucial to suppress the ^{1}H–^{1}H homonuclear dipolar couplings, because otherwise the ^{13}C–^{1}H interaction will be a featureless, many-body interaction. If the ^{1}H–^{1}H coupling is suppressed, however, the ^{13}C will be interacting only with one or several close ^{1}H neighbours, and there will be much more inherent structure in the ^{13}C–^{1}H interaction.

PHILOSOPHICAL TRANSACTIONS OF THE ROYAL SOCIETY A MATHEMATICAL, PHYSICAL & ENGINEERING SCIENCES

This inherent structure has information about ^{13}C–^{1}H distances and angles with respect to the external magnetic field. The chemical shift interaction also has angular information embedded in it, so that if one can do an experiment with a period of dipolar evolution and a period of chemical shift evolution, one can correlate these two interactions to produce both internuclear distances and angles with respect to the chemical shift principal axis system, even in polycrystalline materials.

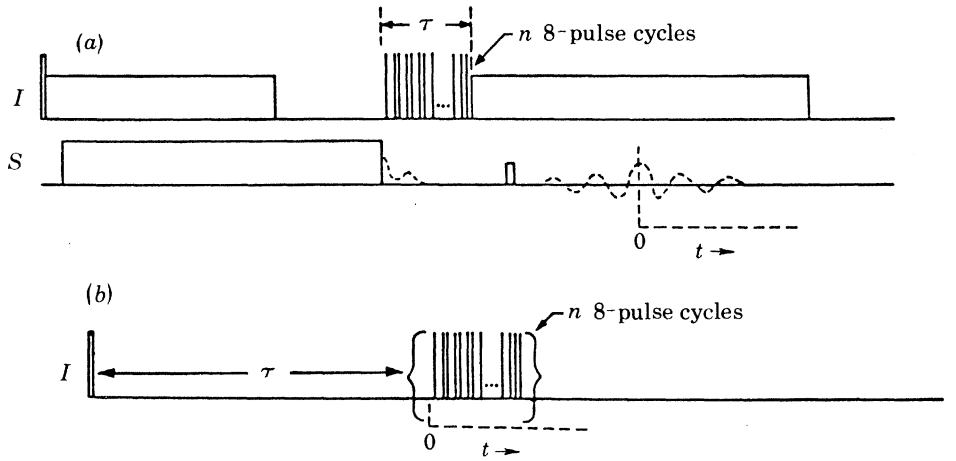

FIGURE 1. Pulse sequences used in dipolar modulated chemical shift spectra experiments (Stoll *et al.* 1976*b*).
(*a*) Schematic of heteronuclear dipolar r.f. sequence. A 90° pulse is applied to the *I* spins and then long cross-polarizing pulses are applied to both *I* and *S* spins. A period of dipolar contact between *I* and *S* spins follows, during which the *I* spins are decoupled by a series of 8-pulse cycles. Then the *I* spins are decoupled from the *S* spins and a 180° pulse is applied to the *S* spins to refocus chemical shift and off-resonance effects creating an echo. The transient decay is acquired from time $t = 0$.
(*b*) Schematic of homonuclear dipolar r.f. sequence. A 90° prepulse is given and followed by the period of dipolar evolution, τ. From time $t = 0$, the 8-pulse cycle is applied to the protons to remove the homonuclear dipolar interaction and the signal is acquired in the windows of the sequence as usual.

The initial dipolar oscillation experiments in Vaughan's laboratory were carried out by Stoll *et al.* (1976*a*, *b*, 1978*a*). It was realized that one should be able to modulate chemical shift spectra with homonuclear as well as heteronuclear dipolar interactions, so there were actually two initial sets of experiments performed, one to demonstrate each principle. Figure 1 shows the r.f. pulse sequences used for both schemes. In figure 1*a* we see the r.f. sequence used for heteronuclear dipolar modulation. First one applies a 90° pulse to the *I* spins and then spin-locking and cross-polarizing pulses applied to both *I* and *S*. This is just a convenient way of making *S* magnetization that takes advantages of the inherent sensitivity benefits of cross-polarizing. After a short time we turn off the long *S* pulse and allow *I*–*S* interaction while applying a series of 8-pulse cycles to eliminate *I*–*I* interaction. During this period the *S* spins are interacting with only one or a few near-neighbour *I* spins. The *S* spins are not interacting with each other because we chose a system where *S* spins are quite dilute, and in general the *S* spins will be ^{13}C or ^{15}N, which have a small magnetogyric ratio. After a time τ we turn off the 8-pulse cycles and decouple the *I* and *S* spins. We then apply a 180° pulse to the *S* spins to refocus chemical shifts and resonance offsets, creating an echo, which we acquire, starting time at $t = 0$. This echo pulse is crucial to experiments on polycrystalline samples, because chemical shift anisotropy is in general so large that there would otherwise be no signal left. The decay at $t = 0$ is a decoupled, chemical shift spectrum, but the period of dipolar contact modifies the 'initial conditions'.

Figure 2 shows heteronuclear dipolar modulated ^{13}C benzene chemical shift spectra. The benzene is frozen and polycrystalline, with each benzene ring having a single site enriched to about 90% ^{13}C. The spectra on the left are experimental while the ones on the right are theoretically synthesized. The spectra are for values of dipolar contact time $\tau = 0, 100, 200, 300, 400, 500\,\mu s$. Note that the spectrum for $\tau = 0$ is just a typical axially symmetric powder pattern. The benzene is frozen, but not cold enough to freeze out the spinning about its sixfold axis, which gives

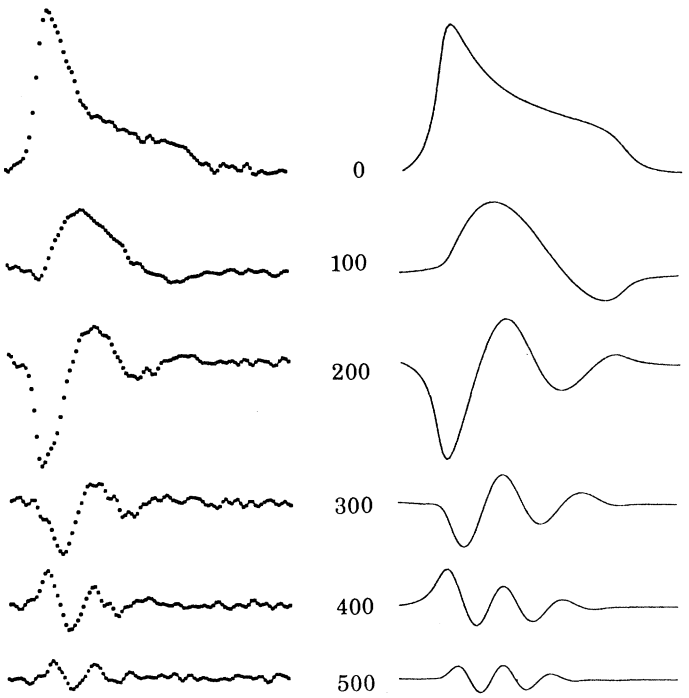

FIGURE 2. Experimental (left) and theoretical (right) heteronuclear dipolar modulated chemical shift spectra in benzene, taking all six protons into account. The spectra are for values of the dipolar modulation time, τ, of 0, 100, 200, 300, 400 and 500 μs from top to bottom. Each channel in the experimental plots is 3.45×10^{-6} for the horizontal scale (Stoll *et al.* 1976*b*).

rise to the axial symmetry. Each point on the chemical shift spectrum corresponds to a locus of orientations of benzene molecules with respect to the magnetic field. Each orientation then experiences a ^{13}C–^{1}H dipolar interaction of a given frequency, which causes each point to linearly oscillate at a particular frequency. The reason that they linearly oscillate is because the average Hamiltonian between the I and S spins during the I–S dipolar contact interval τ is

$$\left.\begin{aligned} \bar{H}_{IS}^{(0)} &= \sum_i \sum_j \tfrac{1}{3}\alpha B_{ij}\,(I_{zi} + I_{xi})\,S_{zj}, \\ B_{ij} &= (\gamma_i \gamma_j / r^3)\,(1 - 3\cos^2\theta_{ij}), \end{aligned}\right\} \tag{20}$$

where α is the chemical shift scaling factor (Haeberlen 1976) and i and j are summed over all I and S spins respectively. This Hamiltonian is of the generic form $I_z S_z$, which, as we saw in §2*a* leads to linear oscillations. Now one could extract dipolar information from any such experiment where $\bar{H}_{IS}^{(0)} \neq 0$, but the linear oscillation leads to particularly simple results in a case like benzene, where we have one S spin and six I spins (Stoll 1976*b*). In this case the correct dipolar oscillation is just a product of cosines of the six separate dipolar frequencies, leading to dipolar frequencies

that are just sums and differences of all six. The six I spins all experience just a single dipolar frequency due to the S spin and cannot even sense the other I spins.

If we do all the mathematics correctly, we compute the transient S magnetization from time $t = 0$ to be

$$\left.\begin{aligned} \langle S_x \rangle &= \sum_j \prod_{i=1}^{6} \sin(\Omega_{ji}\tau) \sin\{\sigma j_{zz}\omega_0 + \Delta\omega)\, t\}, \\ \langle S_y \rangle &= \sum_i \prod_{i=1}^{6} \cos(\Omega_{ji}\tau) \sin\{\sigma j_{zz}\omega_0 + \Delta\omega)\, t\}, \\ \Omega_{ji} &= \tfrac{1}{3\sqrt{2}}\alpha B_{ji}, \end{aligned}\right\} \tag{21}$$

where j is summed over all S spins and i is taken as a product over all six I spins in benzene. Figure 2 shows the theoretically computed spectra based on a value of ^{13}C–^{1}H bond length of 1.09 Å,† which gave the best agreement and is also the generally accepted bond length in benzene. This gives strikingly good agreement with experiment and shows that one can extract such geometrical information even in polycrystalline samples.

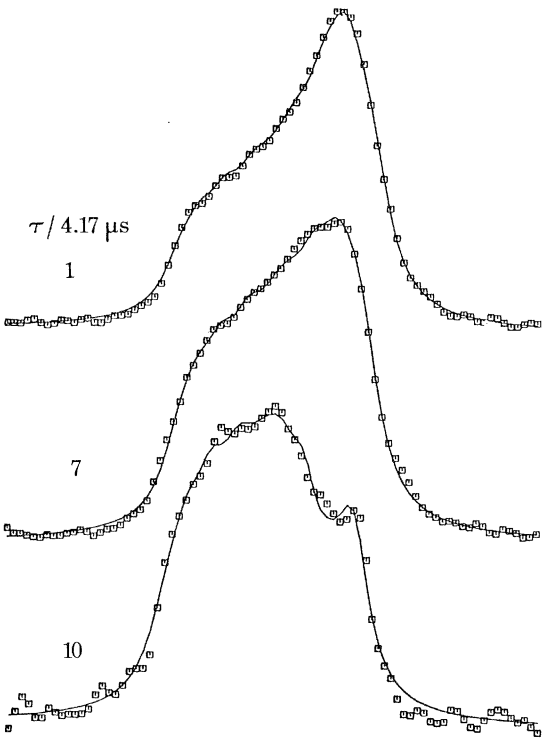

FIGURE 3. Experimental (points) and theoretical (solid) TCAA comparison of homonuclear dipolar modulated chemical shift spectra. The numbers represent values for τ in units of 4.17 μs. On the horizontal axis, each channel is 0.71×10^{-6}. Spectra for $\tau = 7$ and $\tau = 10$ have been magnified vertically by factors of 2 and 5, respectively. (Stoll *et al.* 1978*a*.)

Figure 1*b* shows the r.f. sequence for the homonuclear version of the dipolar modulation experiment (Stoll *et al.* 1976*b*, 1978*a*). Here a 90° prepulse makes I magnetization, which then evolves during a time interval τ under both homonuclear dipolar and chemical shift interactions. The dipolar interaction is then shut off while an 8-pulse sequence is applied. The resulting high-resolution chemical shift spectra are then recorded for various modulation times τ.

† 1 Å = 10^{-10} m = 10^{-1} nm.

Figure 3 shows data from polycrystalline trichloroacetic acid (TCAA), which dimerizes to form relatively well isolated proton pairs. The numbers to the left of the spectra indicate the dipolar evolution time τ in units of 4.17 μs. Using average Hamiltonian theory similar to §2*a*, we synthesized the theoretical curves in figure 3, which agree well with the experimental data. We cannot go into further details here, but it was possible to measure accurate bond lengths and angles in this system as well (Stoll *et al.* 1978*a*).

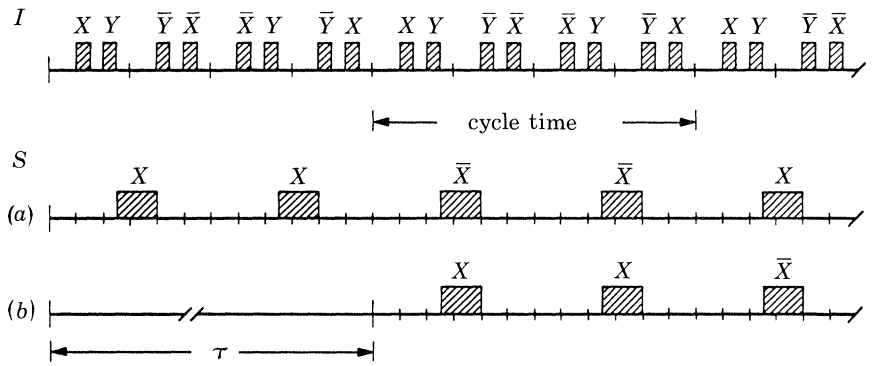

FIGURE 4. Schematic diagram showing *S* spin π pulses properly timed to eliminate accumulation of pulse errors. *X* and $\bar{X}$ refer to the relative phase of the r.f. pulse with $\bar{X}$ being 180° out of phase with *X*. The 8-pulse cycle applied to the *I* spins consists entirely of $\frac{1}{2}\pi$ pulses with relative phases as shown. A delay of the start of the *S* spin π pulse decoupling scheme is shown in (*b*) and produces heteronuclear dipolar-modulated chemical shift spectra (Reimer & Vaughan 1980).

Reimer & Vaughan (1979) have recently developed an experiment that can selectively observe chemical shift spectra from *I* spins coupled to *S* spins. A variation of this experiment has allowed them to do selective dipolar oscillations also (Reimer & Vaughan 1980). The pulse sequence for these experiments is shown in figure 4. An 8-pulse sequence is applied to the *I* spins to remove homonuclear broadening and give high-resolution chemical shift spectra. On alternate scans, 180° pulses are applied to the *S* spins in appropriate windows of the 8-pulse cycle to decouple *I* and *S* spins. These alternate scans are then subtracted to give a difference spectrum. The part of the spectrum due to *I* spins not near *S* spins is unaffected by the 180° *S* pulses, and so the subtraction removes it. On the other hand, the part of the spectrum due to *I* spins coupled to *S* spins is very much affected by the 180° pulses. Without them, the *I*–*S* interaction is so large compared with the *I* chemical shift interaction that the spectrum of *I* spins close to *S* spins is broadened into the baseline. With the 180° pulses, though, the *I*–*S* interaction is removed and one observes the chemical shift spectrum of all the *I* spins. Subtraction of these two spectra then yields a high resolution spectrum of only the *I* spins strongly coupled to *S* spins. Figure 4*a* shows these 180° pulses, while figure 4*b* shows the case when the *S* r.f. is not turned on for a time τ. This case (*b*) will lead to selective spin dipolar modulation. Delaying the decoupling pulses enables the *I* and *S* spins to interact for a time τ and modulate the chemical shift spectra just as in the experiments described earlier in this section. Subtraction of spectra taken with alternately no *S* pulses and delayed *S* pulses will give the selective dipolar oscillations.

Figure 5 shows a selective chemical shift spectrum from only the amide proton of acetanilide, $(C_6H_5)CONHCH_3$. This was taken by using a sample enriched to 95% ^{15}N, and using the technique described above for $I = {}^1H$ and $S = {}^{15}N$. The goal was to observe the chemical shift tensor of hydrogen in an N—H...O hydrogen bond. Although there has recently been interest

in a number of hydrogen-bonded chemical shifts in O—H...O systems, there had been no studies with nitrogen involved in the bonding. Values of the chemical shielding tensor are reported to be $\sigma_1 = 4.6 \times 10^{-6}$, $\sigma_2 = -13.0 \times 10^{-6}$, $\sigma_3 = -13.1 \times 10^{-6}$ with respect to TMS (Reimer & Vaughan 1980).

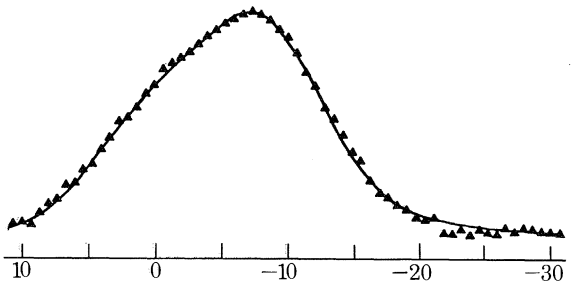

FIGURE 5. Selective proton observed chemical shift spectra for the amide proton in acetanilide $(C_6H_5)CO^{15}NHCH_3$ (Reimer & Vaughan 1980).

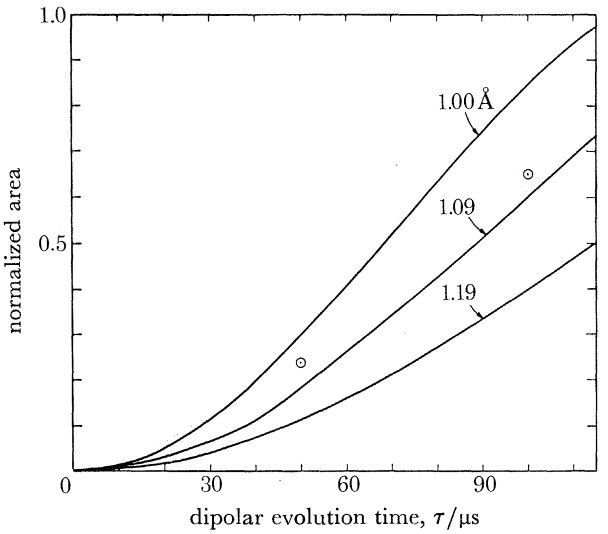

FIGURE 6. Relative area of the dipolar difference spectrum as a function of dipolar evolution time, τ. The curves show three different values of N—H bond lengths. The two open circles show the data points for the N—H...O hydrogen bond in acetanilide and yield an N—H distance of 1.046 ± 0.007 Å (Reimer & Vaughan 1980).

Figure 6 shows a theoretical and experimental comparison of the areas of the selective dipolar oscillation difference spectra from the amide proton as a function of dipolar contact time τ. This area technique was previously shown to be quite accurate for determining internuclear distances, although one can extract no angular information from it (Stoll *et al.* 1976*b*). Three theoretical curves are plotted for N—H distances of 1.00, 1.09 and 1.19 Å. The experimental points correspond to an N—H distance of 1.046 ± 0.007 Å (Reimer & Vaughan 1980).

Duncan and coworkers have used many double-resonance and infrared techniques to study species adsorbed on catalytic surfaces (Duncan 1980; Duncan *et al.* 1980; Duncan & Vaughan 1980; Yates *et al.* 1979*a*, *b*, *c*). One example of this is shown in figure 7, which is a selective dipolar difference spectrum, similar to the one above, of the carbonyl proton of formic acid (HCOOH) adsorbed on ammonium-Y zeolite. The chemical shielding here is reported to be -12.3×10^{-6}

relative to TMS (Duncan & Vaughan 1980; Duncan 1980). This value indicates that carbonyl hydrogen is more acidic than was previously thought and may be more susceptible to nucleophilic attack; this knowledge is crucial in attempting to unravel complicated catalytic reactions.

Figure 8 shows the areas of the selective dipolar oscillation spectra for the same carbonyl proton of formic acid on zeolite (Duncan & Vaughan 1980; Duncan 1980), as well as previously measured dipolar oscillation data for benzene and calcium formate (Stoll *et al.* 1976*b*). The initial decrease of the spectral area for both calcium formate and the surface formate is less than predicted for a 1.09 Å bond length. This slower decrease for calcium formate has been attributed to librational motions in the calcium formate. It appears as though a similar motion may be taking place in the adsorbed formate. For longer dipolar evolution times τ, indirect ^{1}H–^{1}H coupling through ^{1}H–^{27}Al–^{1}H (from ^{27}Al in the zeolite) may contribute enough spin diffusion to cause the area to remain roughly constant.

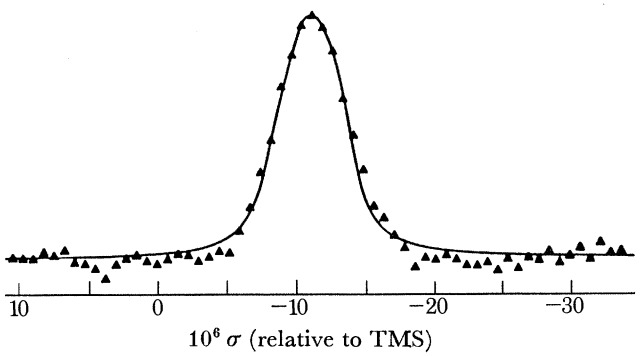

FIGURE 7. Proton spectrum of the carbonyl hydrogen of formic acid adsorbed on the NH_4-Y zeolite at 295 K, obtained with about 8000 averages of the dipolar difference experiment (Duncan & Vaughan 1980; Reimer & Vaughan 1980).

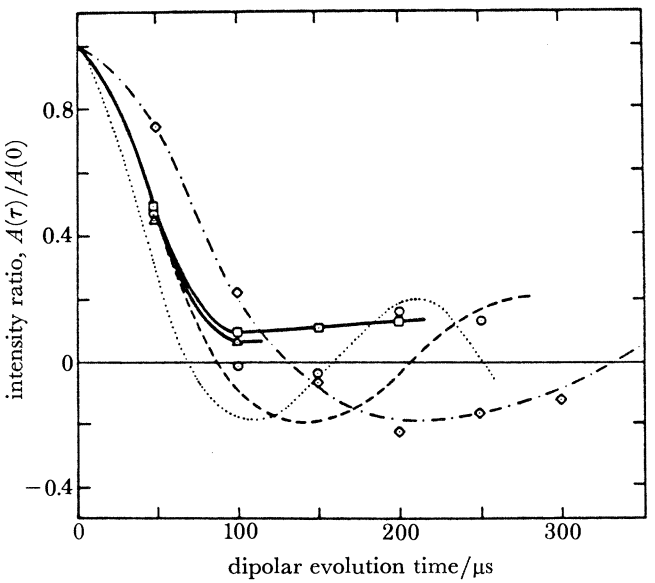

FIGURE 8. Spectral area plotted against the dipolar–modulation time for formic acid adsorbed on the NH_4-Y zeolite at 295 K (□) and at 125 K (△). For comparison, I also plot the data for benzene at 185 K (◇) and calcium formate at 295 K (○) reported previously (Stoll *et al.* 1976*b*). Theoretical curves are for a rigid ^{13}C–^{1}H bond length of 1.09 Å (dotted line), and for a 1.09 Å bond averaged by rotation in a plane (dashes and dots) (Duncan & Vaughan 1980).

3. Phase interferometry

(a) *Background and theory*

In this section we present briefly the theory behind phase-interferometric n.m.r. experiments. There have been a variety of double resonance experiments done over the years that deal with a multiple-level quantum system whereby the populations of certain levels are changed or inverted by selective irradiation of the system. Examples include the nuclear Overhauser effect (1953), electron–nuclear double resonance (Endor) (Pake & Estle 1973), and others. These all deal with populations of quantum states and therefore the diagonal elements of the density matrix. We now consider systems in which we create off-diagonal density matrix elements or transverse magnetization with a well defined phase coherence and then selectively irradiate certain transitions to alter the observable phase of the magnetization.

The most elemental n.m.r. interferometry theory requires three quantum mechanical states, ϕ_1, ϕ_2 and ϕ_3. These states are not degenerate and the corresponding transition frequencies ω_{12}, ω_{23} and ω_{13} are all assumed to be inequivalent. We can write the general wavefunction $\psi(t)$ as

$$\psi(t) = C_1(t)\,\phi_1 + C_2(t)\,\phi_2 + C_3(t)\,\phi_3, \tag{22}$$

where the $C_i(t)$ are the complex amplitudes of the system to be found in the various states ϕ_i. We assume the following initial conditions

$$\left.\begin{aligned} C_1(0) &= 1, \\ C_2(0) &= C_3(0) = 0, \end{aligned}\right\} \tag{23}$$

which means that the system is in the state ϕ_1 at time $t = 0$. Next we create quantum mechanical phase coherence between levels 1 and 2 by applying radiation at the resonant frequency ω_{12}. We must be careful in this thought experiment not to disturb the 1–3 or 2–3 transitions. For sake of simplicity we assume that this radiation is a 90° pulse, which means that after the pulse our system has equal probability of being in ϕ_1 or ϕ_2. Another assumption that we are making is that we are in the interaction frame of the Hamiltonian giving rise to the energy level spacing, and we will therefore not observe any phase oscillations due to this Hamiltonian.

After the 90° pulse we have 'new' initial conditions, indicated by primes:

$$\left.\begin{aligned} C_1'(0) &= C_2'(0) = \tfrac{1}{\sqrt{2}}, \\ C_3'(0) &= 0. \end{aligned}\right\} \tag{24}$$

Our system is now in a quantum state that is a linear combination of ϕ_1 and ϕ_2. Furthermore, there is a definite phase coherence between these states. Since the C_i are complex numbers, we can write them in the form

$$\left.\begin{aligned} C_1 &= A_1 \mathrm{e}^{\mathrm{i}\alpha}, \\ C_2 &= A_2 \mathrm{e}^{\mathrm{i}\beta}, \\ C_3 &= A_3 \mathrm{e}^{\mathrm{i}\gamma}, \end{aligned}\right\} \tag{25}$$

where the A_i are strictly real and positive magnitudes of the complex numbers, and α, β, γ are the phases.

Next we apply a second pulse of radiation to only the 2–3 transition, by irradiating at ω_{23}. After a time t of this irradiation, our coefficients are

$$\left.\begin{aligned} C_1(\tau) &= \tfrac{1}{\sqrt{2}}, \\ C_2(\tau) &= \tfrac{1}{\sqrt{2}}\cos(\Omega\tau), \\ C_3(\tau) &= \tfrac{1}{\sqrt{2}}\sin(\Omega\tau), \end{aligned}\right\} \tag{26}$$

where Ω is a constant depending on the amplitude and other details of the radiation. Since application of this second pulse does not change the phase of C_1, we can observe the change in phase of C_2 by comparison of the phase difference of C_1 and C_2 at time $t = 0$ and later at time $t = \tau$. Thus we have created phase coherence between levels 1 and 2 and modified it by irradiating the 2–3 transition. The coefficient C_1 serves as our reference in the detection of changes in the phase of C_2. The basis of all interferometric experiments is that one cannot observe the overall phase of a quantum mechanical wavefunction, but one can observe relative phases of such wavefunctions.

The other point that we must consider is how we actually use C_1 as our reference for C_2. We do this by observing the expectation value of some operator that connects ϕ_1 and ϕ_2. In the experiments to follow, this is always the transverse nuclear magnetization, but in principle any off-diagonal operator would be suitable. The result is that our expectation value will be proportional to the product $C_1 C_2^*$ and its complex conjugate. Thus we actually measure the quantity $A_1 A_2 \cos(\alpha - \beta)$, which enables us to clearly see how the phase of C_2, which is β, has changed. For (26) this means that we will observe that the 1–2 transverse magnetization is proportional to $\frac{1}{2}\cos(\Omega\tau)$, which leads to linear oscillations. This kind of linear oscillation, which arises from quantum mechanical probabilities, should not be confused with the linear oscillations in §2*a*, which arose from statistical probabilities.

We can now see the intimate connection between the phase that we associate with observables and the phase of a quantum mechanical wavefunction. The phase of an observable connecting two quantum states is just the phase difference between the quantum mechanical amplitudes to be in those two states. The phase of the transverse magnetization is simply the difference between the phases of the amplitudes to be found in adjacent Zeeman spin levels. Similarly in optics, the phase of the electric field is merely the difference between the phase of the amplitudes to be in states of n and $(n \pm 1)$ photons.

This ability to change the phase of a magnetization by selective irradiation of a different transition is the basis for the experiments to be discussed. This gives us a very sensitive way of indirectly detecting a transition frequency by monitoring the phase of a magnetization that corresponds to a different transition. The key to the technique is that we must have two separate quantum transitions with one level in common.

(*b*) *Experiments*

The first phase interferometric n.m.r. experiments performed were those of Stoll *et al.* (1977*a*, *b*). These experiments were done on a prototypical liquid A–X spin system (^{13}C–^{1}H) where both I and S equalled $\frac{1}{2}$. These experiments were undertaken for several reasons. One was to demonstrate spinor character of a two-level system, which means that if a 360° pulse is applied to a two-level system, the overall phase of that two-level system changes by only 180°. A second goal of these experiments was to measure the coherence relaxation times (T_2) of off-diagonal matrix elements corresponding to magnetic dipole forbidden transitions. It was also realized, however, that phase interferometry is an ideal way to detect transitions indirectly, which are difficult to detect directly owing to low frequency or excessive broadening, by observing the phase reversal of a second transition, which is easily detected because of higher frequency or less broadening.

The A–X spin system chosen for these first experiments was 91 % ^{13}C-enriched sodium formate ($NaCHO_2$) dissolved in D_2O with a small amount of HDO as impurity. The ^{1}H and ^{13}C are weakly coupled by a scalar or J coupling, and their energy levels are as shown in figure 9. The allowed ^{1}H transitions between levels 1–3 and 2–4 are inequivalent owing to the presence of the

PHILOSOPHICAL TRANSACTIONS OF THE ROYAL SOCIETY A MATHEMATICAL, PHYSICAL & ENGINEERING SCIENCES

scalar coupling of the form $JI \cdot S$, where J is the coupling constant (195 Hz in this system), as are the ^{13}C transitions 1–2 and 3–4.

In figure 10 we see the r.f. pulsing scheme employed in these experiments. First a strong, non-selective 90° pulse was applied to both ^{1}H transitions (1–3 and 2–4), and then a weak, selective pulse of varying lengths was applied to only *one* of the ^{13}C transitions (1–2). Finally a 180° strong, non-selective pulse was applied to both ^{1}H transitions to create an echo which was then digitized and Fourier-transformed. This 180° pulse was strictly for convenience to avoid loss of signal and linear phase errors and had nothing to do with the interferometry.

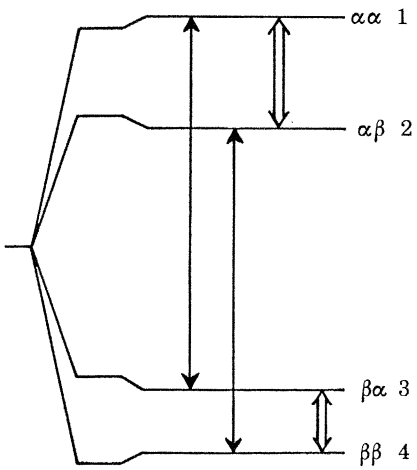

FIGURE 9. Energy levels diagram for an A–X spin system. The α and β represent the two eigenstates spin up and spin down of the spin ½ particle. The first Greek letter represents the state of the ^{1}H spin and the second represents the state of the ^{13}C spin, so that two ^{1}H transitions are shown with single arrows, while the two ^{13}C transitions are shown with double arrows. The numbers 1, 2, 3, 4 are used to refer to the various energy levels or to the eigenstates to which they correspond. The relative Zeeman energies for ^{1}H (56.4 MHz) and ^{13}C (14.2 MHz) have been drawn to scale, but the effects of the weak coupling have been greatly exaggerated for emphasis (Stoll *et al.* 1977*a*).

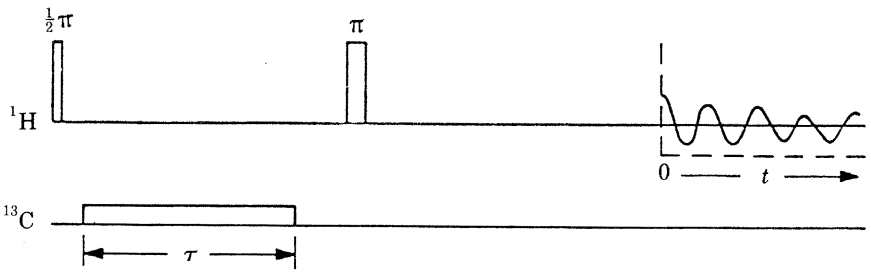

FIGURE 10. Radio-frequency pulse sequence used in phase interferometry experiment. A $\frac{1}{2}\pi$ pulse is applied to both ^{1}H transitions. Then a selective pulse of length τ is applied to only one of the ^{13}C transitions. A π pulse is then applied to both ^{1}H transitions at a time ΔT after the $\frac{1}{2}\pi$ pulse. The signal is recorded from $2\Delta T$ ($t = 0$), defined to be the middle of the echo for Fourier transformation (Stoll *et al.* 1977*b*).

Recall from § 3*a* that to do n.m.r. interferometry we need two inequivalent transitions with one level in common. From the level diagram in figure 9 we see two such three-level systems. One is composed of levels 1–2–3 and the other is 1–2–4. The effect of the 90° pulse in figure 10 is to create phase coherence between levels 1–3 and 2–4. As we saw in § 3*a*, the phase of the transverse magnetization from the 1–3 transition is equal to the difference of the quantum mechanical amplitudes of the spins to be in states 1 and 3. The selective pulse applied to the 1–2 transition

changes both the magnitude and phases of the amplitudes to be in the 1 and 2 states. By observing the 1–3 transition we can use the phase of level 3 as a reference to see how the weak pulse has changed the phase of level 1. Similarly, observing the 2–4 transition with 4 as our reference we see phase changes from 2. Thus the interferometry is done by observation of the phase of the ^{1}H signals.

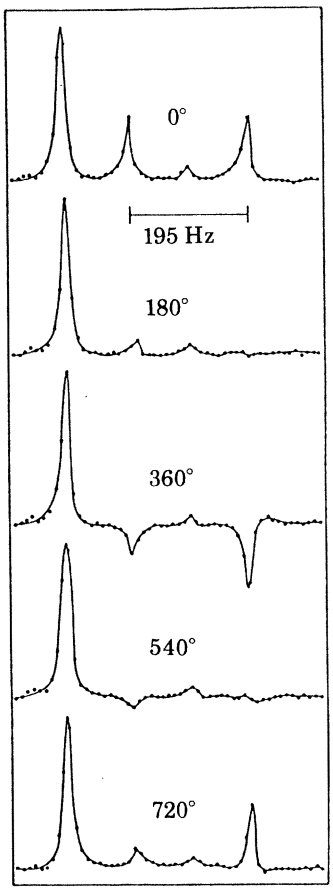

FIGURE 11. Proton phase interferometric spectra for different values of τ. The doublet split by 195 Hz is due to the ^{1}H coupled to the ^{13}C in those formate ions containing ^{13}C. The small peak at the centre of the doublet is due to the ^{1}H in the formate ions containing spinless ^{12}C, while the large peak on the far left is due to the small amount of ^{1}H impurity in the solvent. The five spectra are for values of τ = 0, 28, 56, 84 and 112 ms, corresponding to values of $\omega_1\tau$ = 0°, 180°, 360°, 540° and 720° (Stoll *et al.* 1977*b*).

The effects of the weak pulse can be clearly seen in figure 11. Here is a series of ^{1}H spectra taken for values of 0°, 180°, 360°, 540° and 720° for the length of the selective ^{13}C pulse. For 0° the spectrum is just the usual free-induction decay spectrum. At the far left the large line is impurity HDO in the sample. The second and fourth lines from the left are the 1–3 and 2–4 doublet split by a value of J = 195 Hz. The small peak between the doublet is from the 9 % of the ^{1}H in formate ions containing spinless ^{12}C. When the ^{13}C pulse is 360° then the 1–2 levels experience a phase change of 180°, which demonstrates the spinor character of the 1–2 two level system. This 180° phase change shows up in the ^{1}H spectrum as an inversion of the doublet. Only after a full 720° does the 1–2 level experience a 360° rotation which makes the ^{1}H doublet upright again.

PHILOSOPHICAL TRANSACTIONS OF THE ROYAL SOCIETY A MATHEMATICAL, PHYSICAL & ENGINEERING SCIENCES

One immediately notes from figure 11 that the initially symmetric doublet does not remain symmetric as one might suppose. This is due to relaxation effects (T_2) of off-diagonal density matrix elements corresponding to forbidden transitions. Note that for pulses of 180° and 540° the doublet vanishes. This is reminiscent of the entropy discussion of §2*a*. As in the double-resonance cases discussed there, our magnetization is disappearing but the order is being transferred to off-diagonal density matrix elements, which are non-observable and correspond to forbidden transitions. During the long, weak ^{13}C pulse the order is being passed back and forth, so the T_2 of the 1–4 and 2–3 forbidden transitions play a major role. Because $T_{2(1-4)}$ and $T_{2(2-3)}$ are different, the two members of the doublet do not remain symmetric. Thus from this series of spectra one can measure T_2 of these forbidden transitions. Many interesting off-resonance and relaxation effects were studied in this system but I shall not discuss them further here (Stoll *et al.* 1977*b*).

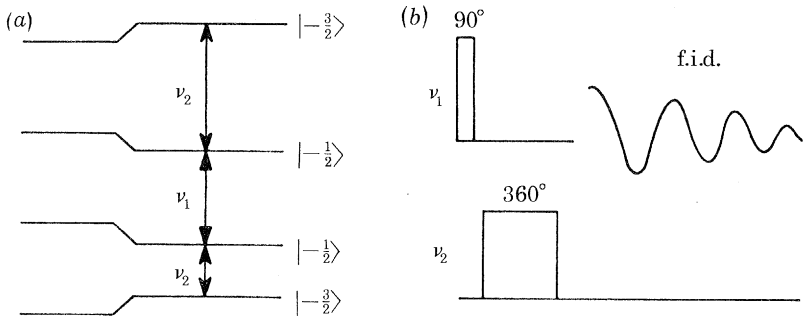

FIGURE 12. (*a*) The first-order quadrupole-shifted energy levels of spin $\frac{3}{2}$ nucleus in a strong magnetic field. (*b*) The pulse sequence used (90°(ν_1)–360°(ν_2)) for the interferometric double-resonance experiment. A 360° pulse is applied at frequency ν_2 to a satellite transition 2–3 μs after a 90° pulse is applied at frequency ν_1 to the central transition (Polak & Vaughan 1977).

The concept of indirect detection in this experiment should be briefly stressed. By observing the inversion of the ^{1}H signal, the ^{13}C transition was indirectly detected. Furthermore, the detection of that ^{13}C transition was made with the sensitivity, resolution, and relaxation time, of the ^{1}H signal. This therefore represents a powerful tool for detecting weak and broad signals by observing a stronger, narrower signal. Furthermore, unlike many indirect detection schemes that may cause a small change in the observed spectra, we have a full 200% change or inversion in the spinor experiments. This phase interferometric scheme is also applicable whenever we have a system with two or more inequivalent transitions having one quantum level in common. It could be applied to systems consisting of coupled nuclear spins, coupled electron and nucleus, or nuclei with a quadrupole interaction. Subsequent works of Wolff and coworkers have explored detailed spin dynamics of phase interferometry in a spin-1, three-level system (Wolff & Mehring 1979; Wolff *et al.* 1979; Mehring *et al.* 1979, 1980; Stoll *et al.* 1978*b*).

This concept of indirect detection was successfully applied by Highe and coworkers to the study of ionic conductors (Polak *et al.* 1977, 1978, 1980; Highe & Vaughan 1978; Highe *et al.* 1979; Vaughan *et al.* 1979). There has been much interest in ionic conductors because of their potential use in energy systems and their unusual physical property of electrical conduction by charge transport of highly mobile ions rather than electrons. One of the more scrutinized of these ionic conductors has been β-alumina. Na and Li have been found to be ions that can conduct electricity and diffuse almost freely within the β-alumina. There have been studies of ^{23}Na in β-alumina

looking at the quadrupolar effects of this spin $\frac{3}{2}$ nucleus; however, nobody was able to observe the first-order quadrupolar broadened wings of the ^{23}Na even in a single crystal of β-alumina.

Figure 12*a* shows the quantum level structure for the ^{23}Na spin $\frac{3}{2}$ nucleus. For a spin $\frac{3}{2}$ system, the $(\frac{1}{2}, -\frac{1}{2})$ transition is usually somewhat sharp because the first-order quadrupole interaction shifts the $\frac{1}{2}$ and $-\frac{1}{2}$ levels the same way, leaving a narrower line that is broadened by second-order quadrupole interactions. However, the $(\frac{3}{2}, \frac{1}{2})$ and $(-\frac{3}{2}, -\frac{1}{2})$ satellite transitions are usually severely broadened, even in single crystals, by first-order quadrupole interactions. In the experiments described here, however, Polak & Vaughan (1977) were able to map these broad satellites by using phase interferometry and indirect detection of the satellites by observation of the sharp central transition.

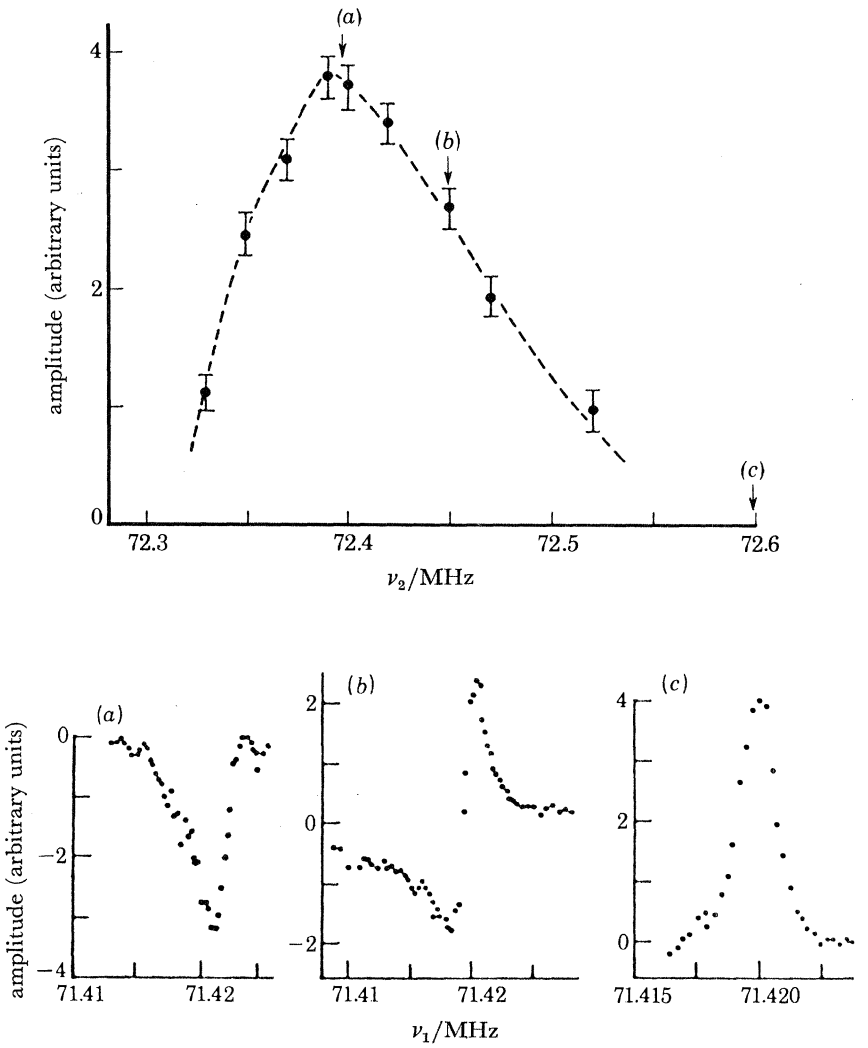

FIGURE 13. Interferometric difference spectrum of the ^{23}Na upfield satellite in β-alumina. The frequency-dependent amplitude represents the intensity of the signal obtained after Fourier transformation of the time-averaged difference between the f.i.d. following a $90°(\nu_1)$–$360°(\nu_2)$ sequence and the f.i.d. following a $90°(\nu_1)$ pulse. H_0 is perpendicular to the β-alumina conduction plane for these results. The three spectra of the central transition (*a*, *b*, *c*) illustrate the phase effects induced by the $90°(\nu_1)$–$360°(\nu_2)$ sequence. Note that the vertical axis of the three spectra has been scaled for presentation (Polak & Vaughan 1977).

The r.f. sequence used for the phase interferometry in ^{23}Na is shown in figure 12*b*. Initially a 90° pulse is applied to the sharp central line at a frequency ν_1. Then a 360° pulse is applied to one of the broad satellite lines at a frequency ν_2. The ensuing free-induction decay (f.i.d.) is then stored. The 90° pulse ensures phase coherence between the $\frac{1}{2}$ and $-\frac{1}{2}$ levels. The 360° applied to the $(\frac{3}{2}, \frac{1}{2})$ transition cause a 180° phase change of the $\frac{3}{2}$ and $\frac{1}{2}$ levels, and hence the relative phase of the $\frac{1}{2}$ and $-\frac{1}{2}$ levels change by 180° and the sharp central line is inverted. Thus one can map the broad satellites by looking at the inversion of the central transition.

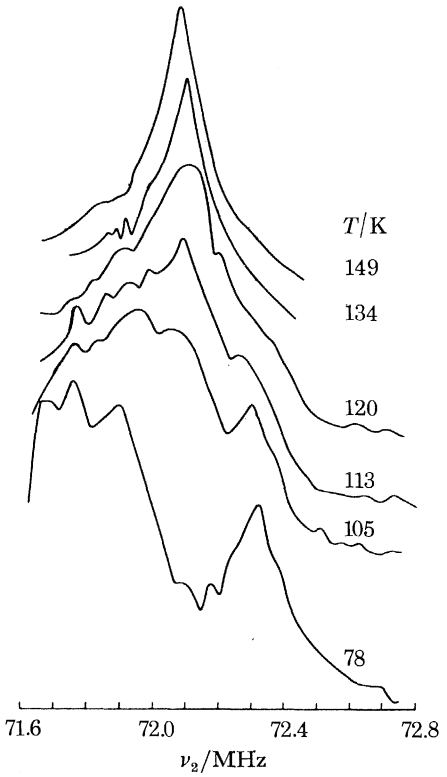

FIGURE 14. Satellite spectra of ^{23}Na in β-alumina obtained with the interferometric amplitude method as a function of temperature. The $\frac{1}{2} \leftrightarrow -\frac{1}{2}$ transition is located at 71.42 MHz, and $H_1 \approx 21$ kHz (Highe *et al.* 1979).

Figure 13 shows such an indirectly detected spectrum. The actual data consisted of plotting the amplitude of the Fourier-transform of the difference of the f.i.ds with and without the 360° pulse, as a function of the frequency of the 360° pulse. Thus the data are a difference spectrum and the difference is greatest when the satellite is being irradiated at its centre. The insets in figure 13 show the central line at three frequencies of 360° pulse. Note that near the centre of the satellite the central transition is inverted, whereas far off the satellite, no inversion of the central line is observed. By using this technique it was possible to determine the lineshape and splitting of the satellites. Although I shall not go into further details, the workers were able to measure quadrupole coupling constants for the ^{23}Na at several different orientations of a single crystal of β-alumina (Polak & Vaughan 1977).

Work done to study the motional properties in β-alumina had previously been able to observe only averages over all sites. Further work with interferometry on ^{23}Na in β-alumina as a function of temperature, however, proved to be a way to separate details of motion not obtainable in any

other way (Highe *et al.* 1979). Figure 14 shows indirectly detected spectra of one of the broad satellites of ^{23}Na in β-alumina taken at various temperatures. It is well known in n.m.r. that spectral lines due to several sites can coalesce when the rate of hopping between the sites becomes comparable to the frequency separation of the lines. Using this reasoning, one can deduce the onset of several different motions at about 120 and 149 K. I shall not go into further details here, but it is possible to estimate the hopping rates and the workers have speculated on details of the actual motional processes by appealing to structural information about the various available sites in the β-alumina (Highe *et al.* 1979). It is important to note that the series of temperature variable spectra in figure 14 not only give dynamical information, but they also contain quadrupolar splittings that can be used to assign particular sites as well as reliable spectral areas that can be used to assign populations of various sites at various temperatures.

Two-dimensional spectroscopy has been used to correlate first- and second-order quadrupolar interactions (Polak *et al.* 1980). Since these two are averaged differently by motion, this may prove to be a fruitful area of pursuit. It might also be possible to correlate chemical shift or dipolar data with quadrupolar data to extract geometrical information in polycrystalline materials, similar to the dipolar oscillations discussed in § 2 *b*.

4. Conclusions

Double-resonance interactions have been shown theoretically to lead to only four kinds of behaviour of the magnetization: no behaviour (decoupling), precession, linear oscillation and transfer (cross-polarizing). Average Hamiltonian theory seems to be a useful way to calculate the behaviour of *I*–*S* spin systems for pulsed or c.w. experiments. Dipolar oscillation of chemical shift spectra, both heteronuclear and homonuclear, have been able to measure structural and motional information in polycrystalline materials. Dipolar difference experiments, as well as many other double-resonance techniques, have been applied to a variety of systems, including species adsorbed on catalytic surfaces. The dipolar difference experiment allows one to examine selectively one specific site even if there are a variety of different sites in the material.

Phase-interferometric experiments are applicable to systems having more than one inequivalent transition with one level in common. The advantages of interferometric indirect detection for weak or broad transitions have been shown. With these techniques one can obtain compositional and motional information in quadrupolar systems unobtainable by conventional means. Phase interferometry has been used to study relaxation for forbidden transitions.

All of these techniques are still relatively recent and they have yet to become well known and widely applied in the n.m.r. community. These techniques vary in difficulty from the complicated dipolar oscillation experiments to the simpler phase-interferometric experiments. It remains to be seen how useful these techniques may become; however, early results indicate that these techniques, in particular the interferometric techniques with their wide range of applicability to many solid and liquid spin systems, both nuclear and electron, should be further investigated.

In these areas, as well as other areas of n.m.r., Bob Vaughan and his colleagues have played an important role. He will be missed.

The author would like to acknowledge willing assistance with figures from and invaluable discussions with Dr A. J. Vega, Dr T. M. Duncan, Dr M. Polak, Professor M. Mehring, Dr J. A. Reimer, Dr A. Highe and, of course, the late Professor R. W. Vaughan.

PHILOSOPHICAL TRANSACTIONS OF THE ROYAL SOCIETY A MATHEMATICAL, PHYSICAL & ENGINEERING SCIENCES

References (Stoll)

Aue, W. P., Bartholdi, E. & Ernst, R. R. 1976 *J. chem. Phys.* **64**, 2229.

Duncan, T. M. 1980 Ph.D. thesis, California Institute of Technology, Pasadena.

Duncan, T. M. & Vaughan, R. W. 1980 *J. chem. Phys.* **73**, 975.

Duncan, T. M., Yates, J. T. & Vaughan, R. W. 1980 *J. Catal.* (Submitted.)

Freeman, R. & Anderson, W. A. 1962 *J. chem. Phys.* **37**, 2053.

Haeberlen, U. 1976 *High Resolution NMR in solids: selective averaging*. New York: Academic Press.

Haeberlen, U. & Waugh, J. S. 1968 *Phys. Rev.* **175**, 453.

Hartmann, S. R. & Hahn, E. L. 1962 *Phys. Rev.* **128**, 2042.

Hester, R. K., Cross, V. R., Ackerman, J. L. & Waugh, J. S. 1975*b* *J. chem. Phys.* **63**, 3606.

Hester, R. K., Ackerman, J. L., Cross, V. R. & Waugh, J. S. 1975*a* *Phys. Rev. Lett.* **34**, 993.

Hester, R. K., Ackerman, J. L., Neff, B. L. & Waugh, J. S. 1976 *Phys. Rev. Lett.* **36**, 1081.

Highe, A. & Vaughan, R. W. 1978 *J. chem. Phys.* **69**, 4206.

Highe, A., Polak, M. & Vaughan, R. W. 1979 In *Proceedings, International Conference on Fast Iron Transport in Solids*, Lake Geneva, Wisconsin, 21–25 May (ed. P. Vashishta, J. N. Mundy & G. K. Shenoy), p. 305. Amsterdam: North-Holland.

Magnus, W. 1954 *Communs pure appl. Math.* **7**, 649.

Mehring, M. 1976 *High resolution NMR spectroscopy in solids*. Berlin: Springer-Verlag.

Mehring, M., Stoll, M. E. & Wolff, E. K. 1979 In *Proceedings, XXth Congress Ampere*, Tallinn, U.S.S.R., 21–26 August 1978 (ed. E. Kundla, E. Lippmaa & T. Saluvere), p. 137. Berlin and New York: Springer-Verlag.

Mehring, M., Wolff, E. K. & Stoll, M. E. 1980 *J. magn. Reson.* **37**, 475–495.

Overhauser, W. A. 1953 *Phys. Rev.* **89**, 689.

Pake, G. E. & Estle, T. L. 1973 *The physical principles of electron paramagnetic resonance*, 2nd edn. Reading: Benjamin.

Pines, A., Gibby, M. G. & Waugh, J. S. 1973 *J. chem. Phys.* **59**, 569.

Polak, M. & Vaughan, R. W. 1977 *Phys. Rev. Lett.* **39**, 1677.

Polak, M. & Vaughan, R. W. 1978 *J. chem. Phys.* **69**, 3232.

Polak, M., Highe, A. J. & Vaughan, R. W. 1980 *J. magn. Reson.* **37**, 357–361.

Reimer, J. A. & Vaughan, R. W. 1979 *Chem. Phys. Lett.* **63**, 163.

Reimer, J. A. & Vaughan, R. W. 1980 *J. magn. Reson.* (Submitted.)

Rhim, W. K., Elleman, D. D., Schreiber, L. B. & Vaughan, R. W. 1974 *J. chem. Phys.* **60**, 4595.

Slichter, C. P. 1978 *Principles of magnetic resonance*, 2nd edn. New York: Springer-Verlag.

Stoll, M. E. 1977 Ph.D. thesis, California Institute of Technology, Pasadena.

Stoll, M. E., Vega, A. J. & Vaughan, R. W. 1976*a* *J. chem. Phys.* **65**, 4093.

Stoll, M. E., Vega, A. J. & Vaughan, R. W. 1976*b* In *Proceedings, XIXth Congress Ampere*, Heidelberg, Germany, 27 September – 1 October 1976 (ed. H. Brunner, K. H. Hausser & D. Schweitzer), p. 429. Heidelberg: Groupement Ampere.

Stoll, M. E., Vega, A. J. & Vaughan, R. W. 1977*a* *Phys. Rev.* A **16**, 1521.

Stoll, M. E., Vega, A. J. & Vaughan, R. W. 1977*b* *J. chem. Phys.* **67**, 2029.

Stoll, M. E., Vega, A. J. & Vaughan, R. W. 1978*a* *J. chem. Phys.* **69**, 5458.

Stoll, M. E., Wolff, E. K. & Mehring, M. 1978*b* *Phys. Rev.* A **17**, 1561.

Vaughan, R. W., Polak, M. & Highe, A. 1979 In *Proceedings, XXth Congress Ampere*, Tallinn, U.S.S.R., 21–26 August 1978 (ed. E. Kundla, E. Lippmaa & T. Saluvere), p. 138. Berlin and New York: Springer-Verlag.

Waugh, J. S. 1976 *Proc. natn. Acad. Sci. U.S.A.* **73**, 1394.

Wolff, E. K. & Mehring, M. 1979 *Phys. Lett.* A **70**, 125.

Wolff, E. K., Stoll, M. E. & Mehring, M. 1979 In *Proceedings, XXth Congress Ampere*, Tallinn, U.S.S.R., 21–26 August, 1978 (ed. E. Kundla, E. Lippmaa & T. Saluvere), p. 90. Berlin and New York: Springer-Verlag.

Yates, J. T., Duncan, T. M. & Vaughan, R. W. 1979*c* *J. chem. Phys.* **71**, 3908.

Yates, J. T., Duncan, T. M., Worley, S. D. & Vaughan, R. W. 1979*a* *J. chem. Phys.* **70**, 1219.

Yates, J. T., Worley, S. D., Duncan, T. M. & Vaughan, R. W. 1979*b* *J. chem. Phys.* **70**, 1225.

PHILOSOPHICAL TRANSACTIONS OF THE ROYAL SOCIETY A MATHEMATICAL, PHYSICAL & ENGINEERING SCIENCES